Brazilian Journal
of Chemical
Engineering

ISSN 0104-6632
Printed in Brazil
www.scielo.br/bjce

Vol. 35, No. 03, pp. 869-886, July - September, 2018
dx.doi.org/10.1590/0104-6632.20180353s20170327

MODELING THE CORE METABOLISM OF *Komagataeibacter hansenii* ATCC 23769 TO EVALUATE NANOCELLULOSE BIOSYNTHESIS

Samara Silva de Souza[1], Julia de Vasconcellos Castro[1], and Luismar Marques Porto[1,*]

[1] Chemical and Food Engineering Department, Federal University of Santa Catarina. InteLab - Integrated Technologies Laboratory, Genomic and Tissue Engineering Group. Florianópolis - Santa Catarina, Brazil

(Submitted: June 21, 2017; Revised: August 19, 2017; Accepted: September 1, 2017)

Abstract - Genome-scale metabolic models based on a combination of genome sequence and biochemical information have strongly influenced the field of systems biology. However, basic principles of the operation of metabolic networks, in particular the central metabolism can be easily studied in smaller metabolic (core) models. *Komagataeibacter hansenii* ATCC 23769 has been used for bacterial nanocellulose (BNC) biosynthesis, and the recent availability of its genome sequence allowed the development of a metabolic model. The core metabolic model was constructed from an initial draft metabolic reconstruction including 74 reactions and 68 metabolites that provides insights for a better understanding of *K. hansenii* metabolic pathways. The applicability of the model is finally demonstrated by applying the FBA approach, and the *in silico* simulation successfully predicted the minimal medium and the growing abilities on different substrates. This core model can facilitate system-level metabolic analysis as well as developments for improving BNC production.

Keywords: *Komagataeibacter hansenii*; Bacterial nanocellulose; Core metabolic model; Flux balance analysis.

INTRODUCTION

Metabolic models have a promising ability to describe cellular phenotypes accurately and to relate the annotated genome sequence to the physiological functions of a cell (Covert et al., 2001; Kim et al., 2015). There is an extensive diversity of unexplored metabolism encoded into the genomes of microorganisms and a huge gap in understanding the link between the genetic information and the resulting phenotype (Blank and Ebert, 2013; Mahadevan et al., 2011). Metabolic models are based on a network of chemical reactions that characterize the vast metabolic network of an organism (Almaas et al., 2004; Shimizu, 2009; Wiechert, 2002). These networks may be used to generate metabolic states for a given set of environmental conditions.

Genomes of several bacterial strains have been sequenced and annotated, providing information that has been used alongside biochemical and physiological data to reconstruct metabolic networks (Huang et al., 2014; Loira et al., 2012; Terzer et al., 2009; Zhang and Hua, 2015). A comprehensive protocol was developed to describe each step necessary to build a high-quality genome-scale metabolic reconstruction (Thiele and Palsson, 2010). This protocol was properly structured for large-scale metabolic networks and well-studied organisms when several experimental evidences are available to allow the required significant manual curation (Becker et al., 2007; Cheng et al., 2009). Although

**Corresponding author.* E-mail address: luismar@intelab.ufsc.br

well-curated genome-scale models were developed, some microorganisms do not have sufficient information available about their metabolic features. In this case, reducing those models to a certain core or module while keeping key elements or/and important functional properties, i.e., to construct metabolic core models, can be a suitable way to study and understand basic principles of the central metabolism. In core models, the reactions and pathways are chosen to represent the most well-known and widely studied metabolic pathways (Orth, 2010). However, for the construction of a core and representative model for organisms with little reported information on their metabolic capabilities, some adaptations in the current protocol were necessary.

The combination of metabolic network reconstruction and constraint-based modeling provides a rich information set from which one can build mathematical models of biological interest (Barabási and Oltvai, 2004). Moreover, computational tools have been developed to predict fluxes in biochemical networks, thereby integrating different fields such as systems biology, bioinformatics and metabolic engineering (Fernández-Castané et al., 2014; Ishii et al., 2004; McCloskey et al., 2013). Flux Balance Analysis (FBA) has been successfully applied to obtain growth predictions, theoretical product yields and for a global estimation of flux distribution within the metabolism of different organisms (Grafahrend-Belau et al., 2014; Reed, 2012). Critical steps in FBA are the reconstruction of a metabolic network, followed by mass balance, imposition of constraints, choice of a suitable (biologically relevant) objective function and linear optimization (Angeles-Martinez and Theodoropoulos, 2016; Orth et al., 2010; Raman and Chandra, 2009). Simulation results can be a useful guide for metabolic engineering (Liu et al., 2014; Simeonidis and Price, 2015). Currently, a popular tool for investigating complex metabolic models is the constraint-based reconstruction and analysis (COBRA), a MATLAB(r) (MathWorks Inc.) toolbox (Becker et al., 2007; Schellenberger et al., 2011). Our group has developed a set of computational systems biology tools, called GEnSys (Genomic Engineering System), which comprises several modules that allow analysis and simulation of biochemical reaction networks, for instance, flux balance analysis (FBA) (Bagnariolli et al., 2010).

Komagataeibacter hansenii ATCC 23769 (formerly *Gluconacetobacter hansenii*) (Iyer et al., 2010; Yamada et al., 2012) produces, as a result of the fermentation process, a microstructured nanocellulose with high purity (Benziman et al., 1980; Deinema and Zevenhuizen, 1971; Ross et al., 1991). Bacterial nanocellulose (BNC) is a potential material for medical applications and it has been commonly applied as wound dressing and temporary skin replacement (Cheng et al., 2009; Hutchens et al., 2007; Jorfi and Foster, 2015; Jozala et al., 2016). Given the importance of bacterial nanocellulose-based biomaterials in tissue engineering, an *in silico* core metabolic model of *K. hansenii* can provide new strategic insights into the BNC synthesis and be useful in the study of typical synthesis conditions, such as different growth media, environmental conditions and formation of bioproducts. *K. hansenii* is not the most commonly studied model bacterium for BNC production, such as *K. xylinum*, however it has the ability, as well, to produce nanocellulose (Ramana et al., 2000; Ruka et al., 2012; Zeng et al., 2011).

Here, a core metabolic model of *K. hansenii* ATCC 23769 was developed, based on the draft assembly of the genome of this bacterium (GenBank accession no. CM000920 and taxonomy ID: 714995) (Iyer et al., 2010). Through simulation, relevant physiological scenarios were studied. The FBA approach was performed to simulate different conditions and maximize specific reactions to understand the effects of nanocellulose production and distribution of cellular fluxes by varying three carbon sources: glucose, mannitol and glycerol under minimal nutritional requirements. These carbon sources were chosen because they are known to lead to differences in the nanocellulose microstructure, which have different fiber densities (Mikkelsen et al., 2009; Ruka et al., 2012). This *in silico* model can facilitate system-level metabolic analysis and allow experiments with *K. hansenii* growing in a defined medium that enables controlled experiments since the exact composition of nutrients is known.

MATERIALS AND METHODS

Draft reconstruction

The reconstruction process of the *K. hansenii* core metabolic model involved the following steps, as outlined in Figure 1: (1) creation of a draft model (draft reconstruction); (2) reconstruction of a detailed model (manual curation to build the core model); (3) conversion into a mathematical format (FBA; mathematical formulation); (4) analysis of the network (model simulation).

The annotated data of the draft genome sequence of *K. hansenii* (NCBI ID 714995; ACCESSION NZ CM000920, 3636659 bp) (Iyer et al., 2010) were used in two different platforms that can map genes to reactions in an automated manner and allow exporting all reactions and metabolites to a SBML file, to create two different drafts models. The first one was the software Pathway

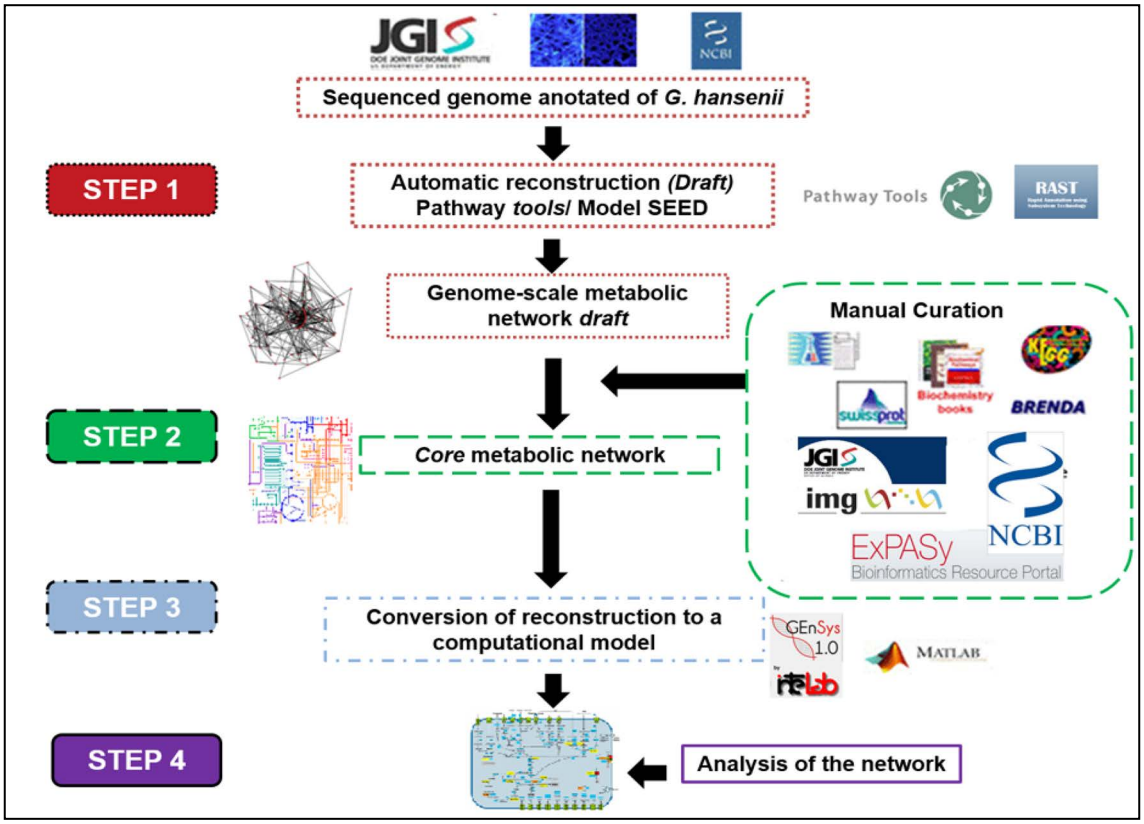

Figure 1. Schematic illustration of the network reconstruction. The four steps used in the present work are: 1) creation of a draft model using automated resources, 2) manual curation to construct the core model, 3) conversion of the model into a mathematical format and, 4) biological analysis of the network through simulations.

Tools (SRI International), version 16.5 (Karp et al., 2002, 2009; Paley et al., 2012) that gives a raw draft model file as a result. The second one was the web-based resource, called Model SEED (Devoid et al., 2013), where the assembled genome sequence is annotated by the RAST server, which provides a semi-automated curation of the draft model. The set of reactions from the drafts contains incorrect or unbalanced stoichiometry, missing reactions and mistakes from the annotated sequence and neither of these approaches replace a careful manual curation. The resources used during the reconstruction are summarized in Table 1.

Manual curation

The basic principles of the operation of metabolic networks, in particular of the central metabolism, can sometimes be more easily studied in smaller scale models, known as core models (Hädicke and Klamt, 2017). As the goal is to construct a core model that represents the central metabolism of *K. hansenii* in detail, the reactions and metabolites involved in glycolysis, pentose phosphate pathway, Entner-Doudoroff pathway, tricarboxylic acid cycle, and key reactions of the electron transport chain were included in the model. To improve network connectivity and decrease the number of dead-end metabolites, the reactions not inferred in the automatic drafts models were added during manual curation. Such reactions include: (1) spontaneous reactions; (2) extracellular transport reactions; (3) intracellular transport reactions; and (4) exchange reactions, which allows specific molecules through the system and environment and (5) reactions of cellulose biosynthesis common to microorganism producers.

Biochemistry textbooks and biochemical digital databases, including KEGG (Kanehisa et al., 2006, 2010), BRENDA (Scheer et al., 2011), ExPASy (Gasteiger et al., 2003) and the platform IMG (Integrated Microbial Genomes) (Markowitz et al., 2012) were used to verify the reactions. A biochemical thermodynamics calculator, eQuilibrator (Flamholz et al., 2012), was used to check the reversibility and stoichiometry of the reactions. The metabolic reactions in the model were organized into two compartments (cytoplasm and extracellular) based on the localization of associated enzymes. Then, we organized the reactions into pathways/subsystems. For each metabolite, the charge, formula and identification were compiled from the KEGG database.

The last step was the incorporation of a biomass reaction. In order to represent growth, the core *K. hansenii* model includes a biomass reaction, which drains precursor

Table 1. Online resources for the reconstruction of the metabolic network of K hansenii.

RESOURCE	URL
Genome sequence (NCBI)	http://www.ncbi.nlm.nih.gov/genome/?term=gluconacetobacter%20hansenii
IMG – Integrated Microbial Genomes	http://img.jgi.doe.gov/cgi-bin/w/main.cgi
Kyoto Encyclopedia of Genes and Genomes	http://www.genome.jp/kegg/pathway.html
ExPASy Biochemical Pathways	http://www.expasy.ch/cgi-bin/search-biochem-index
BRENDA	http://www.brenda-enzymes.org
Uniprot	http://www.uniprot.org/uniprot/?query=gluconacetobacter%20hansenii&sort=score
SEED	http://pubseed.theseed.org
eQuilibrator	http://equilibrator.weizmann.ac.il
SBML validator	http://sbml.org/validator
MATLAB®	http://www.mathworks.com
Pathway Tools version 16.5	http://bioinformatics.ai.sri.com/ptools
COBRA (Constraint-based reconstruction and analysis) toolbox	http://opencobra.sourceforge.net/openCOBRA/Welcome.html
GNU linear programming toolkit (GLPK)	http://glpkmex.sourceforge.net
SBMLToolbox version 4.0.1	http://www.sbml.org
libSBML library 4.0.1	http://sbml.org/Software/libSBML
rBioNet	http://sourceforge.net/projects/opencobra/files/cobra/foundry/rBioNet
GEnSys	Available upon request from the authors.

metabolites from the network. The biomass composition data for *K. hansenii* used in this study was obtained from the literature (Edirisinghe et al., 2016). The reaction of the biomass included internal protons and water (Appendix - Table A1). The amount of water required is equal to the amount of hydrolyzed ATP to satisfy the ATP growth requirement. The ATP hydrolysis results in the production of one proton, while using NADPH as NADH consumes one proton, resulting in the production of protons in the biomass reaction. All precursors were added to the molecules to perform oxidation (NAD), reduction (NADPH) and provide energy (ATP), resulting in 1 mol of biomass, which is the amount of biomass produced with these compounds. Missing reactions (referred to as gaps) that resulted in dead-end metabolites and prevented the computational simulation of cell growth were identified and filled in. The procedure was continued until all the biomass components were include. This ensures that the reduced network contains at least all protected reactions and, additionally, a set of biosynthesis routes that produces all components consumed by the biomass synthesis reaction. In total, 74 reactions and their reactants have been protected in the central metabolism as listed in the Appendix (Tables A1 and A2).

The *in silico* minimal medium composition capable of supporting growth of *K. hansenii* chosen was the Yamanaka medium (Yamanaka et al., 1989), which is composed of 50 $g \cdot L^{-1}$ (carbon source), 5 $g \cdot L^{-1}$ (nitrogen source) and 3 $g \cdot L^{-1}$ (phosphate source). Three different carbon sources (glucose, mannitol and glycerol) were used to calculate the carbon flux through different pathways. The uptake rates of nitrogen and phosphate sources were determined according to the composition of the medium and we used experimental data in continuous culture since the FBA approach assumes steady state and generates predictions that are consistent with continuous culture. Biomass concentration and dilution rate values were estimated to calculate and infer the maximum uptake rates of nitrogen ($(NH_4)_2SO_4$) and phosphate sources (KH_2PO_4) in the model.

Flux Balance Analysis (FBA)

The metabolic flux distribution of the core model of *K. hansenii* was calculated using FBA. With this approach, it was possible to obtain the optimal solution for the intracellular fluxes by optimizing an objective function. The core model was converted into a mathematical representation known as a stoichiometric matrix. The stoichiometric matrix (S) consists of rows of metabolites and columns of reactions, and is the basis from which all constraints-based modeling is carried out. The converted core model is expressed as a stoichiometric model represented by a pseudo steady-state system of mass balance equations $dc/dt = S \cdot v = 0$, where v corresponds to a vector of all reaction fluxes in the network (Feist, 2009; Orth et al., 2010). To identify optimal solutions in the vast solution space, we defined FBA objective functions to solve the system of linear equations that represent the mass balance constraints. In this study, we evaluated four scenarios for biologically meaningful predictions: (i) maximization of biomass yield; (ii) maximization of nanocellulose synthesis, product of greatest interest derived from the bacterium *K. hansenii*; (iii) the maximization of the external metabolites to evaluate the balance consistency; and (iv) the ability to synthesize precursors of biomass by adding demand reactions. Moreover, metabolic flux distribution was estimated under limitations of some nutrients, such as phosphate and nitrogen source.

The constraints for the upper and lower bounds of reversible and irreversible reactions were defined as $-\infty \leq v_i \leq \infty$ and $0 \leq v_i \leq \infty$, respectively. For irreversible reactions, the lower bound was set to zero and for reversible reactions, lower and upper bounds were typically set to arbitrarily large values. Besides defining the directions of all metabolic reactions, these constraints were used to specify a maximum flux through a given reaction or to specify a measured substrate uptake rate. Exchange reactions were added to enable uptake and secretion of extracellular metabolites for simulations. The stoichiometry and the reversibility of each reaction, together with the steady state assumption for the internal metabolites, allow defining a region of feasible flux distribution.

Model simulation

The core metabolic network of *K. hansenii* was built and loaded into MATLAB® (MathWorks Inc.) using functions available in the GEnSys toolbox (Bagnariolli et al., 2010). The GenSys Toolbox is available upon request. By using Flux Balance Analysis (FBA), we investigated the core metabolic network of *K. hansenii* through simulations. The flux values were expressed in $mmol \cdot gDW^{-1} \cdot h^{-1}$. For the simulation of aerobic growth on minimal medium, we allowed the following external metabolites to freely enter and leave the network: O_2, H^+, CO_2, H_2O, NH_4^+ and PO_4^{3-}. With the minimal medium, each carbon source was allowed to enter into the *in silico* core model one by one by adding exchange reactions (if there was no corresponding one) for the sake of simulating the growth under different environmental conditions.

The core metabolic model construction is an integrated process. Through experimentally determined biochemical characteristics of *K. hansenii* combined with computer modeling provided advances to understand what happens inside a cell through *in silico* simulation (Figure 2).

From the annotated genome sequence, a core metabolic model of *K. hansenii* was constructed to comprehend the mechanisms and synthesis of bacterial nanocellulose. This core model can facilitate system-level metabolic analysis as well as developments for improving BNC production.

RESULTS AND DISCUSSION

Metabolic model reconstruction

The initial draft of the core reconstruction was built from the annotated genome of *K. hansenii* ATCC 23769. The chromosomal sequence contains 3,547,122 bp, with a GC content of 59%. The genome contains 3,351 genes, of which 3,308 are protein-encoding genes, accounting for 84% of the genome. There are 43 genes for tRNAs and two rRNA loci. The genes encoding proteins involved in cellulose synthesis are in operons consisting of *acsAB* (GXY_04277; GXY_08864), *acsC* (GXY_04282; GXY_08869) and *acsD* (GXY_04292). The two drafts generated by Pathway Tools and Model SEED were initial mapping processes that list the rough data of the metabolites and reactions of this organism. They were stored in both SBML and XLS formats and were used to manage all the consolidated data.

From a topological analysis, a metabolic network can be interpreted as a bipartite graph, consisting of two sets of nodes that represent metabolites and reactions, respectively. The two disjoint sets of nodes are connected by a set of (directed or undirected) edges, specifying which metabolites participate in a reaction. This graph represents the visualization of the stoichiometric matrix, known as sparse matrix, since most of the coefficients are zero (Figure 3).

Our results revealed a sparsity matrix, with 4,703 zero elements which correspond to 93.5% of sparsity. The non-zero (nz) elements or null space correspond to the density of the matrix, which is this case represents 6.5%

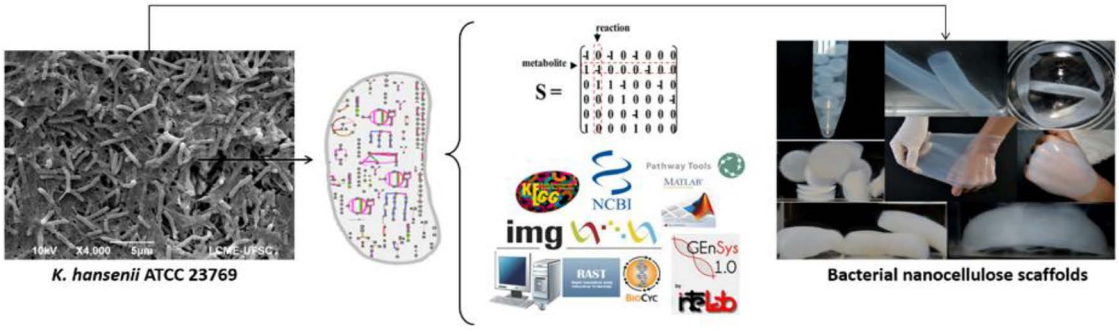

Figure 2. Biochemical analysis and computer modeling to advance the understanding of what happens inside a cell. The core metabolic network is modified in the context of other physiological constraints to produce a mathematical model, which can be used to generate quantitatively testable hypotheses in silico. Depending on the culture conditions, *K. hansenii* is able to synthesize BNC with different shapes, such as membranes, spheres and vessels.

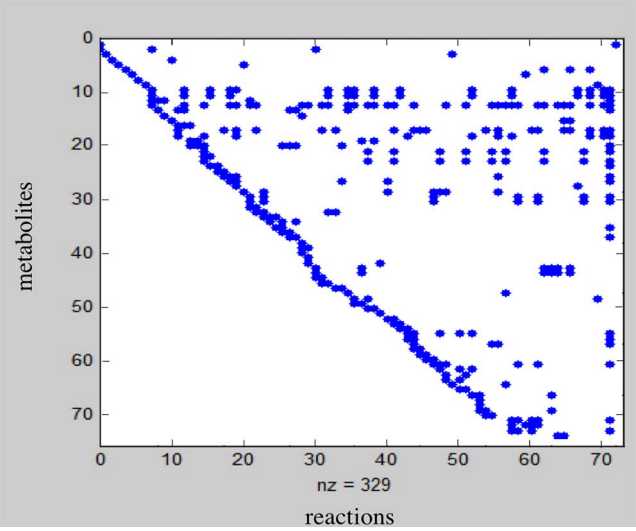

Figure 3. Sparse matrix of the K. hansenii core model. The matrix contains 329 non-zero elements (blue points), with 4,703 zero elements (white points). Its sparsity is 93.5%, and its density is 6.5%.

(nz=329). A sparsity matrix indicates that most substrates participate in only a few reactions, whereas a small number of metabolites, such as ATP, NADPH, NADH, participate in a very large number of reactions. These more interconnected metabolites play important roles in the metabolic network: for example, the stability in the transport of such metabolites inside or outside the network can affect the organization of regulatory mechanisms. Generally, metabolic networks are considered to be sparse and sparsity has been used as a criteria for inferring linear network models.

In silico capabilities of the *K. hansenii core* metabolic model

Model simulations were carried out to obtain insights on the metabolic network and the flux distribution. The metabolic flux analysis combines a set of measured fluxes (often extracellular), with a constraint-based model to obtain an estimate of all the fluxes. In this case, the uptake and consumption rates for all three carbon sources and for nitrogen and phosphate sources were set, as shown in Table 2.

The network contains 79 metabolites and 74 fluxes. Of those, 68 are internal metabolites, resulting in 6 degrees of freedom and the stoichiometric matrix consisted of 68 rows and 74 columns. The matrix included exchange reactions to allow metabolites to be taken up or excreted to the extracellular medium, and transport reactions to allow the uptake of metabolites. Because the number of measured fluxes is less than the degrees of freedom of the matrix, the solution space will have infinite solutions. To determinate the optimal solution, an objective function was used to obtain a linear programming problem. The four physiological scenarios of interest were defined as objective functions: (i) maximization of biomass yield; (ii) maximization of nanocellulose synthesis; (iii) maximization of the external metabolites; and (iv) the ability to synthesize precursors of biomass by adding demand reactions. Each objective function was tested with the addition of constraints (Table 2) to identify which one was the most appropriate for predicting fluxes by FBA.

With the FBA technique, the carbon sources were chosen to evaluate the capability of *K. hansenii* to grow on each carbon source supplemented in the minimal medium. Glucose and mannitol uptake rates were 10 $mmol \cdot gDW^{-1} \cdot h^{-1}$ and glycerol uptake rate was 20 $mmol \cdot gDW^{-1} \cdot h^{-1}$. Uptake rates were established based on the C-mol of each carbon source. Glucose and mannitol are six-carbon sources, while glycerol is a three-carbon source. The rates were obtained by dividing the concentration ($g(L^{-1})$) of each source by its molar mass ($g(mol^{-1})$), and then multiplying it by the specific dilution rate (h^{-1}) divided by biomass concentration ($g_{DW}(L^{-1})$). Also, for the correct mass balance of the model, glycerol needed to enter twice as much as the other carbon sources.

In order to analyze the metabolic flux for these different carbon sources at the same dilution rate and to prevent the wash out, a dilution rate of 0.05·h was chosen for the experiments, based on previous studies which revealed a high growth yield using a low dilution rate (Olijve and Kok, 1979). For simulation of aerobic growth on Yamanaka medium, the following external metabolites were allowed to freely enter and leave the network: O_2, H^+, CO_2, H_2O, NH_4^+ and PO_4^{3-}, except for the carbon sources. Since the nutrients, such as nitrogen and phosphate, are not considered unlimited, the maximum uptake rates of nitrogen and phosphate were calculated to determine which combination results in an optimal growth of bacterial nanocellulose. A maximum uptake rate of 1.26 $mmol \cdot gDW^{-1} \cdot h^{-1}$ and 0.78 $mmol \cdot gDW^{-1} \cdot h^{-1}$, for nitrogen and phosphate, respectively, were set as lower boundaries ($-1.26 \leq v \leq 1000$ $mmol \cdot gDW^{-1} \cdot h^{-1}$) and ($-0.78 \leq v \leq 1000$ $mmol \cdot gDW^{-1} \cdot h^{-1}$). The oxygen uptake was set as a virtually unlimited flux ($-1000 \leq v \leq 1000$ $mmol \cdot gDW^{-1} \cdot h^{-1}$), because *K. hansenii* is an aerobic bacterium.

The COBRA Toolbox generated the Systems Biology Markup Language (SBML) file of the core model. The XML-based data format is presented in the Supplementary file I "sbml_coremodel". The FBA method computes the maximal growth yield achievable in the core metabolic model by maximizing the biomass reaction flux (v74). By maximizing the biomass reaction (Figure 4) the carbon flux was used for the bacterial growth, without any production of cellulose (reaction v5) (See reactions in the

Table 2. Composition and boundary conditions of the minimal growth medium for the simulations. The carbon source uptake rates were set and the following external metabolites were allowed to freely enter and leave the network. All the equations are from extracellular [e] compartment to the cytoplasm [c].

Reaction description	Equation	LB *	UB *
Carbon Source			
Glucose	[e]: glc-D ->	0	10
Mannitol	[e]: mann ->	0	10
Glycerol	[e]: glyc ->	0	20
O_2exchange	[e]: o_2<->	-1000	1000
H_2O exchange	[e]: h_2o <->	-1000	1000
Proton exchange	[e]: h <->	-1000	1000
NH_4^+exchange (Nitrogen source)	[e]: nh_4<->	-1.3	1000
PO_4^{-3}exchange (Phosphate source)	[e]: pi <->	-0.75	1000
CO_2exchange	[e]: co_2<->	-1000	1000

*LB: lower bound; UB: upper bound; unit are given in mmol·gDW^{-1}·h^{-1}.

appendix - Table A1). This is a biological representative scenario since there are strains that do not produce cellulose (Iguchi et al., 2000).

Flux distribution using glycerol as a carbon source revealed that the pentose phosphate pathway was not favored (Figure 4). The fraction of carbon directed to the pentose phosphate pathway was growth-rate dependent. The specific growth rates per hour were $\mu = 1.93$ in glucose, and lower in mannitol, $\mu = 0.72$ and $\mu = 0.84$ in glycerol, under minimal nutritional requirements. These results indicated that the bacterium has the metabolic machinery needed to use all those carbon sources for growth competence. This is the first reported *in silico* prediction of *K. hansenii* metabolic capabilities under a minimal medium growth condition. We have tested the hypothesis that *K. hansenii* uses its metabolism to grow at a maximal rate using the core metabolic model. Based on this hypothesis, further studies should be performed to describe the quantitative relationship between glucose uptake rate, oxygen uptake rate, and maximal cellular growth rate.

The second scenario was the maximization of nanocellulose synthesis. In this case, we used this reaction of BNC production (v5) as objective function. During the analysis, the results revealed that this flux is a suitable objective function and predicts the theoretical yield of nanocellulose, since the biomass flux (cell growth) was zero under that constraint. Thus, the majority of the carbon flux is directed to the production of nanocellulose, and there was no carbon used to produce biomass. The theoretical nanocellulose yield was calculated per mol of carbon of the substrate consumed: 0.95 C-mol/C-mol of glucose, 0.5 C-mol/C-mol of mannitol and 0.6 C-mol/C-mol of glycerol, on a Carbon-mol base. These results can be explained by the metabolism of *K. hansenii*. Glucose is easily transported through the cell membrane and incorporated into the nanocellulose biosynthetic pathway (Oikawa et al., 1995; Ross et al., 1991). Mannitol is known to be converted to fructose, and then metabolized by this organism to produce BNC, while glucose and fructose are transported through the cell membrane and incorporated into the cellulose biosynthetic pathway. Glycerol, a three-carbon sugar, on the other hand, is introduced into metabolic pathways at the triose phosphate level. The oxidation of triose phosphate is a primary reaction in this organism for the channeling of sugar carbon from the pentose phosphate pathway (PPP) into the tricarboxylic acid cycle (TCA cycle). Biosynthesis of bacterial nanocellulose depends on two amphibolic pathways (anabolism and catabolism): PPP for the oxidation of carbohydrates and TCA for the oxidation of organic acids and related compounds (Brown et al., 1976; Oikawa et al., 1995; Ross et al., 1991).

This could explain the lower theoretical nanocellulose yield using mannitol and glycerol, compared to glucose as carbon source. In terms of BNC yields, there is a variation depending on the strain, the composition of the medium and the operating conditions, such as static or agitated culture, temperature, oxygen and pH (Jozala et al., 2016; Keshk and Sameshima, 2005; Ruka et al., 2012). The core model is consistent with experimental data, since this bacterium can synthesize BNC with all these carbon sources. The central metabolic pathway for the three carbon sources varies in many aspects like the pathway used for catabolism of carbon sources and production of extra-cellular metabolites, as shown in Figure 5.

The inability to metabolize glucose (GLC) via the Embden-Meyerhof pathway in *K. hansenii* lies in the fact that it lacks phosphofructokinase, which is required for glycolysis (Velasco-Bedrán and López-Isunza, 2007; Zhong et al., 2014). Gluconeogenesis occurs from oxaloacetate (OAA) via pyruvate (PYR), because of the unusual regulation of the enzymes oxaloacetate decarboxylase and pyruvate phosphate dikinase. Thus, cellulose arises in this organism from a metabolic pool of hexose phosphate that is sustained directly by the phosphorylation of exogenous hexoses and indirectly via the pentose phosphate and the gluconeogenic pathways.

The glucose catabolism involves its conversion to glyceraldehyde-3-phosphate and pyruvate via the

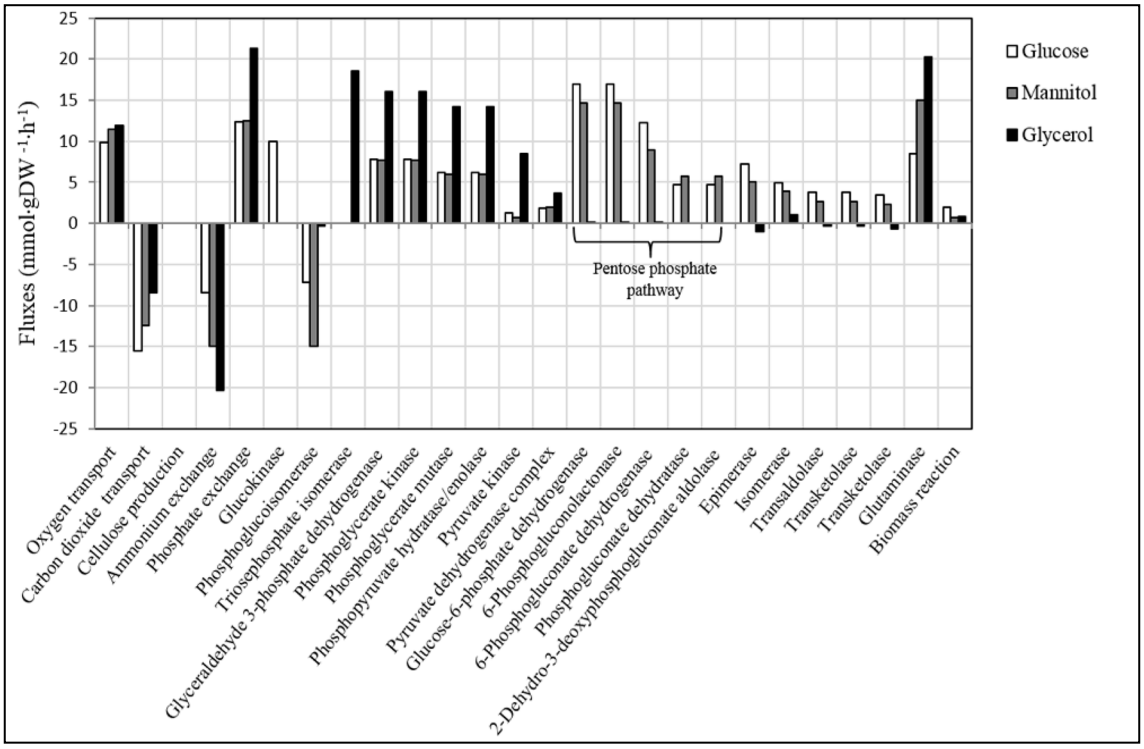

Figure 4. Representation of the most important metabolic fluxes resulting from FBA analysis using the biomass reaction as the objective function. By maximizing this reaction, we proved that all carbon flux was used for bacterial growth without any production of BNC. Glucose as carbon source presented the highest specific growth rates per hour, $\mu = 1.93$. Mannitol and glycerol showed lower growth rates, $\mu = 0.72$ and $\mu = 0.84$, respectively.

Enter-Doudoroff enzymes 6-phosphogluconate dehydrogenase and 2-dehydro-3-deoxyphosphogluconate aldolase. Depending on physiological conditions, glucose is converted into 6-phosphogluconate (6PGC) by one of two routes, one of which is oxidative and the other is phosphorylative. The direct oxidative route involves oxidation of glucose to gluconate (GLCN) and gluconokinase. Alternatively, the phosphorylative route involves uptake of glucose by an inducible transport system. Once inside the organism, glucose is phosphorylated by glucokinase and then converted to 6-phosphogluconate by glucose-6--phosphate dehydrogenase. One important metabolite that influenced the nanocellulose synthesis is the gluconic acid production, which our core model predicted, in accordance with previous studies (Hwang et al., 1999; Ishihara et al., 2002; Liu et al., 2016). Our results showed that the three carbon sources, glucose, mannitol and glycerol can be used by *K. hansenii* under minimal nutritional requirements. To the best of our knowledge, no previous studies reported a core metabolic model of *K. hansenii* ATCC 23769. Two metabolic networks of *Gluconacetobacter xylinus* E25 were developed, the first by Ross (Ross et al., 1991) consisted in 42 reactions, and the second by Zhong and co-workers (Zhong et al., 2013), adapted from Ross' model, consisted of 26 reactions. Zhong and coworkers (2013) performed a metabolic flux analysis (MFA) to compare the metabolic flux distribution. However, neither of these two networks was built based on the genome sequence and a flux balance analysis performed.

The third scenario related to the maximization of external metabolites evaluated the balance consistency. For example, to maximize carbon dioxide (CO2_out), 10 $mmol \cdot gDW^{-1} \cdot h^{-1}$ of glucose was fed, resulting in 60 $mmol \cdot gDW^{-1} \cdot h^{-1}$of CO_2. This is stoichiometrically consistent, given that glucose has six carbons and the carbon dioxide molecule has only one. The mass balance was checked using all external metabolites.

In the fourth scenario, the ability to synthesize precursors of biomass by adding demand reactions was performed. To verify the fluxes distribution under nutrient deprived conditions, nitrogen, phosphate and oxygen uptake were limited, which means those fluxes were set to zero. Under oxygen limitation conditions the bacterial growth rate, nanocellulose production and all the other main function were null, as expected, confirming aerobic functionality. Limitation of nitrogen and/or phosphate sources was shown to be insufficient to prevent bacterial growth. According to Ross (Ross et al., 1991), in *Acetobacter xylinum* washed cells, deprived of a nitrogen source, production of nanocellulose continues when supplied with an adequate carbon substrate and does not depend on net protein synthesis. The excess of available

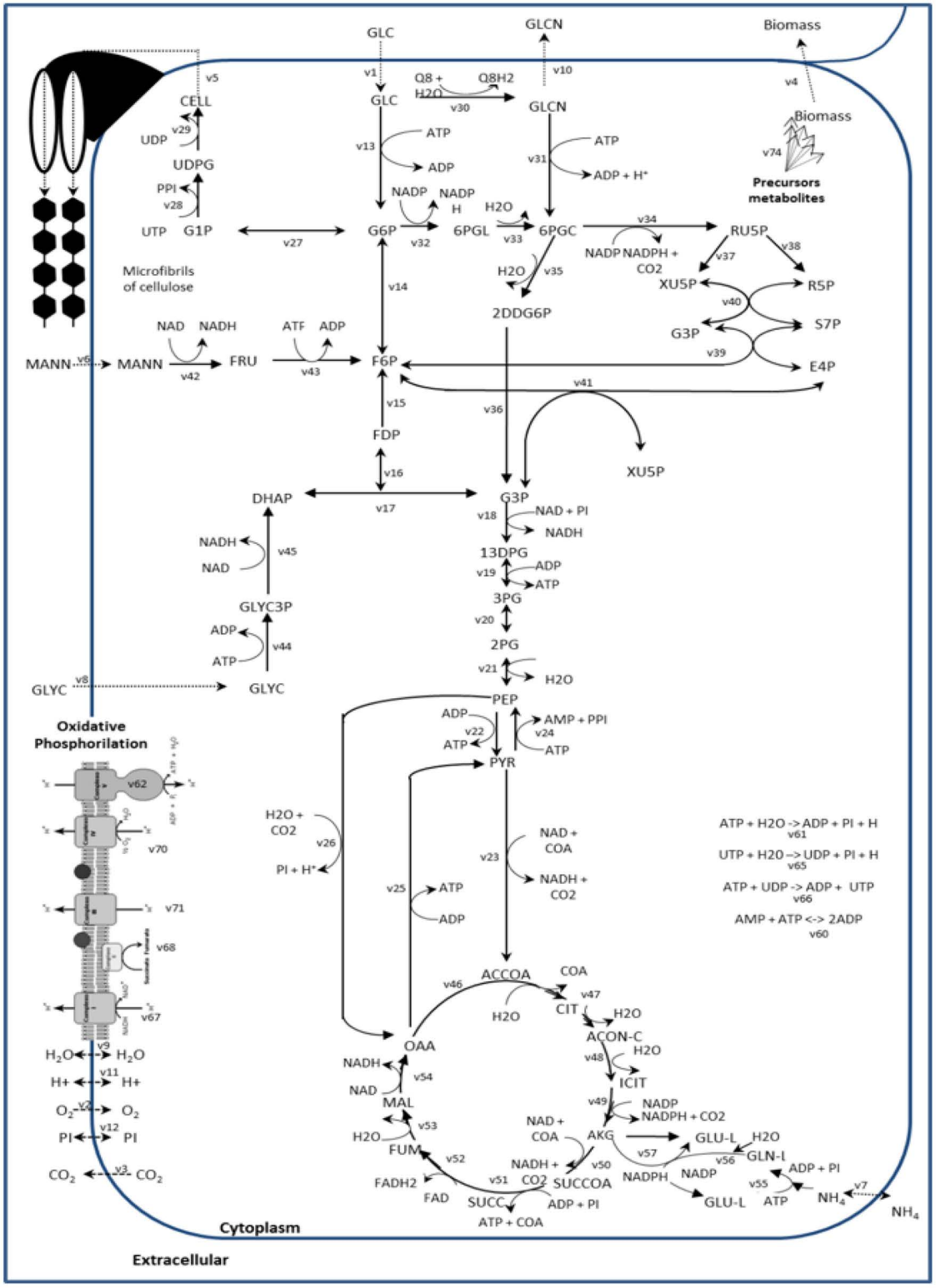

Figure 5. Representation of the core metabolic network of *K. hansenii* and the input of three carbon sources: glucose (GLC), mannitol (MANN) and glycerol (GLYC). The microfibrils of BNC and biomass are represented as output. Metabolite abbreviations and reaction details are provided in the Appendix (Tables A1 and A2).

carbon substrate and limitations in other nutrients, such as nitrogen or phosphate, could promote nanocellulose synthesis. Flux consistency implies that each one of the metabolite precursors was produced by the bacterium. By including a demand reaction (reaction that consumes the compound without producing anything) for each metabolite of the biomass reaction, and optimizing demand reaction fluxes, results revealed that the core model could predict each of the biomass constituents, for all carbon sources used.

CONCLUSIONS

In this study, a core metabolic model of *K. hansenii* ATCC 23769 was developed. The network was constructed by using automatic reconstruction and an iterative process of manual curation based on genomic and bibliome databases. This curated core model accounts for 68 metabolites and 74 reactions and represents an up-to-date database that encompasses the knowledge available in public databases, scientific publications and textbooks on the metabolism of this bacteria.

Flux balance analysis of the model was applied under different physiological scenarios and predicted quantitative relationships between input rates of nutrients, output rates of products and bacterial growth rate. A simplified model could answer simple biological questions and the central carbon metabolism addressed key metabolites. Moreover, the *in silico* core model successfully predicted the growing abilities on different substrates and gave insights of the use of minimal medium capable to support BNC production. With the increased interest in BNC, the *in silico* model presented here will be a valuable tool for fundamental research, serving as a starting point for metabolic engineering approaches. The core model is one important step for understanding the nanocellulose production process and contributes to the general knowledge of microbial function and physiology with computational analysis.

ACKNOWLEDGEMENTS

This work was supported by the Financer of Studies and Projects - FINEP (grant 550084/2014-2 MCT/ FINEP-COENG), by the Coordination of Improvement of Higher Education Personnel - CAPES (scholarship grant 1118675/2012-1- Samara Silva de Souza) and by the National Council for Scientific and Technological Development - CNPq (grant 402901/2013-4 - MCTI/ CNPq/CT-Biotec and scholarship grant 158853/2012-1 CNPq GM/GD - Julia de Vasconcellos Castro). The content is solely the responsibility of the authors and does not necessarily represent the official views of the funding agencies.APPENDIX

REFERENCES

Almaas, E., Kovacs, B., Vicsek, T., Oltvai, Z. N. and Barabasi, A.-L., Global organization of metabolic fluxes in the bacterium Escherichia coli, Nature, 427(6977), 839-843 (2004).

Angeles-Martinez, L. and Theodoropoulos, C., Estimation of flux distribution in metabolic networks accounting for thermodynamic constraints: The effect of equilibrium vs. blocked reactions, Biochem. Eng. J., 105, Part, 347-357 (2016).

Bagnariolli, B., Oliveira, I. L., Castro, J. de V. and Porto, L. M., GEnSys 1.0 - A Systems Biology Toolbox for Complex Biochemical Reaction Networks, in XVIII Brazilian Congress of Chemical Engineering, Foz do Iguaçu. (2010).

Barabási, A.-L. and Oltvai, Z. N., Network biology: understanding the cell's functional organization., Nat. Rev. Genet., 5(2), 101-113 (2004).

Becker, S. A., Feist, A. M., Mo, M. L., Hannum, G., Palsson, B. O. and Herrgard, M. J., Quantitative prediction of cellular metabolism with constraint-based models: the COBRA Toolbox, Nat. Protoc., 2(3), 727-738 (2007).

Benziman, M., Haigler, C. H., Brown, R. M., White, a R. andCooper, K. M., Cellulose biogenesis: Polymerization and crystallization are coupled processes in Acetobacter xylinum., Proc. Natl. Acad. Sci. U. S. A., 77(11), 6678-6682 (1980).

Blank, L. M. and Ebert, B. E., From measurement to implementation of metabolic fluxes, Curr. Opin. Biotechnol., 24(1), 13-21 (2013).

Brown, R. M., Willison, J. H. and Richardson, C. L., Cellulose biosynthesis in Acetobacter xylinum: visualization of the site of synthesis and direct measurement of the in vivo process., Proc. Natl. Acad. Sci. U. S. A., 73(12), 4565-4569 (1976).

Cheng, K.-C., Catchmark, J. and Demirci, A., Enhanced production of bacterial cellulose by using a biofilm reactor and its material property analysis, J. Biol. Eng., 3(1), 12 (2009).

Covert, M. W., Schilling, C. H., Famili, I., Edwards, J. S., Goryanin, I. I., Selkov, E. and Palsson, B. O., Metabolic modeling of microbial strains *in silico*, Trends Biochem. Sci., 26(3), 179-186 (2001).

Deinema, M. and Zevenhuizen, L. P. T. M., Formation of cellulose fibrils by gram-negative bacteria and their role in bacterial flocculation, Arch. Mikrobiol., 78(1), 42-57 (1971).

Devoid, S., Overbeek, R., DeJongh, M., Vonstein, V., Best, A. and Henry, C., Automated Genome Annotation and Metabolic Model Reconstruction in the SEED and

Model SEED, in Systems Metabolic Engineering SE - 2, vol. 985, edited by H. S. Alper, pp. 17-45, Humana Press. (2013).

Edirisinghe, J. N., Weisenhorn, P., Conrad, N., Xia, F., Overbeek, R., Stevens, R. L. and Henry, C. S., Modeling central metabolism and energy biosynthesis across microbial life, BMC Genomics, 17(1), 568 (2016).

Feist, A. M., Reconstruction of biochemical networks in microorganisms, Nat Rev Microbiol, 7(2), 129-143 (2009).

Fernández-Castané, A., Fehér, T., Carbonell, P., Pauthenier, C. and Faulon, J.-L., Computer-aided design for metabolic engineering, J. Biotechnol., 192, Part, 302-313 (2014).

Flamholz, A., Noor, E., Bar-Even, A. and Milo, R., eQuilibrator-the biochemical thermodynamics calculator, Nucleic Acids Res., 40(Database issue), D770-D775 (2012).

Gasteiger, E., Gattiker, A., Hoogland, C., Ivanyi, I., Appel, R. D. and Bairoch, A., ExPASy: the proteomics server for in-depth protein knowledge and analysis, Nucleic Acids Res., 31(13), 3784-3788 (2003).

Grafahrend-Belau, E., Junker, A., Schreiber, F. and Junker, B., Flux Balance Analysis as an Alternative Method to Estimate Fluxes Without Labeling, in Plant Metabolic Flux Analysis SE - 17, vol. 1090, edited by M. Dieuaide-Noubhani and A. P. Alonso, pp. 281-299, Humana Press. (2014).

Hädicke, O. and Klamt, S. EColiCore2: a reference network model of the central metabolism of Escherichia coli and relationships to its genome-scale parent model. Scientific Reports, v. 7, p. 39647, (2017).

Huang, Y., Zhu, C., Yang, J., Nie, Y., Chen, C. and Sun, D., Recent advances in bacterial cellulose, Cellulose, 21(1), 1-30 (2014).

Hutchens, S. A., León, R. V, O'Neill, H. M. and Evans, B. R., Statistical analysis of optimal culture conditions for Gluconacetobacter hansenii cellulose production, Lett. Appl. Microbiol., 44(2), 175-180 (2007).

Hwang, J. W., Yang, Y. K., Hwang, J. K., Pyun, Y. R. and Kim, Y. S., Effects of pH and dissolved oxygen on cellulose production by Acetobacter xylinum BRC5 in agitated culture, J. Biosci. Bioeng., 88(2), 183-188 (1999).

Iguchi, M., Yamanaka, S. and Budhiono, A., Bacterial cellulose-a masterpiece of nature's arts, J. Mater. Sci., 35(2), 261-270 (2000).

Ishihara, M., Matsunaga, M., Hayashi, N. and Tišler, V., Utilization of d-xylose as carbon source for production of bacterial cellulose, Enzyme Microb. Technol., 31(7), 986-991 (2002).

Ishii, N., Robert, M., Nakayama, Y., Kanai, A. and Tomita, M., Toward large-scale modeling of the microbial cell for computer simulation, J. Biotechnol., 113(1-3), 281-294(2004).

Iyer, P. R., Geib, S. M., Catchmark, J., Kao, T. H. and Tien, M., Genome sequence of a cellulose-producing bacterium, Gluconacetobacter hansenii ATCC 23769, J. Bacteriol., 192(16), 4256-4257 (2010).

Jorfi, M. and Foster, E. J., Recent advances in nanocellulose for biomedical applications, J. Appl. Polym. Sci., 132(14) (2015).

Jozala, A. F., de Lencastre-Novaes, L. C., Lopes, A. M., de Carvalho Santos-Ebinuma, V., Mazzola, P. G., Pessoa-Jr, A., Grotto, D., Gerenutti, M. and Chaud, M. V., Bacterial nanocellulose production and application: a 10-year overview, Appl. Microbiol. Biotechnol., 100(5), 2063-2072 (2016).

Kanehisa, M., Goto, S., Hattori, M., Aoki-Kinoshita, K. F., Itoh, M., Kawashima, S., Katayama, T., Araki, M. and Hirakawa, M., From genomics to chemical genomics: new developments in KEGG, Nucleic Acids Res., 34(suppl 1), D354-D357 (2006).

Kanehisa, M., Goto, S., Furumichi, M., Tanabe, M. and Hirakawa, M., KEGG for representation and analysis of molecular networks involving diseases and drugs, Nucleic Acids Res., 38(suppl 1), D355-D360 (2010).

Karp, P. D., Paley, S. and Romero, P., The Pathway Tools software., Bioinformatics, 18 Suppl 1, S225-S232 (2002).

Karp, P. D., Paley, S. M., Krummenacker, M., Latendresse, M., Dale, J. M., Lee, T. J., Kaipa, P., Gilham, F., Spaulding, A., Popescu, L., Altman, T., Paulsen, I., Keseler, I. M. and Caspi, R., Pathway Tools version 13.0: Integrated software for pathway/genome informatics and systems biology, Brief. Bioinform., 11(1), 40-79 (2009).

Keshk, S. M. A. S. and Sameshima, K., Evaluation of different carbon sources for bacterial cellulose production, African J. Biotechnol., 4(6), 478-482 (2005).

Kim, B., Kim, W., Kim, D. and Lee, S., Applications of genome-scale metabolic network model in metabolic engineering, J. Ind. Microbiol. Biotechnol., 42(3), 339-348 (2015).

Liu, M., Zhong, C., Zhang, Y. M., Xu, Z. M., Qiao, C. S. and Jia, S. R., Metabolic Investigation in Gluconacetobacter xylinus and Its Bacterial Cellulose Production under a Direct Current Electric Field, Front. Microbiol., 7, 331 (2016).

Liu, Y., Shin, H., Li, J. and Liu, L., Toward metabolic engineering in the context of system biology and

synthetic biology: advances and prospects, Appl. Microbiol. Biotechnol., 99(3), 1109-1118 (2014).

Loira, N., Dulermo, T., Nicaud, J.-M. and Sherman, D., A genome-scale metabolic model of the lipid-accumulating yeast Yarrowia lipolytica, BMC Syst. Biol., 6(1), 35 (2012).

Mahadevan, R., Palsson, B. Ø. and Lovley, D. R., In situ to *in silico* and back: elucidating the physiology and ecology of Geobacter spp. using genome-scale modelling, Nat Rev Micro, 9(1), 39-50 (2011).

Markowitz, V. M., Chen, I.-M. A., Palaniappan, K., Chu, K., Szeto, E., Grechkin, Y., Ratner, A., Jacob, B., Huang, J., Williams, P., Huntemann, M., Anderson, I., Mavromatis, K., Ivanova, N. N. and Kyrpides, N. C., IMG: the integrated microbial genomes database and comparative analysis system, Nucleic Acids Res., 40(D1), D115-D122 (2012).

McCloskey, D., Palsson, B. Ø. and Feist, A. M., Basic and applied uses of genome-scale metabolic network reconstructions of Escherichia coli., Mol. Syst. Biol., 9(1), 661 (2013).

Mikkelsen, D., Flanagan, B. M., Dykes, G. a. and Gidley, M. J., Influence of different carbon sources on bacterial cellulose production by Gluconacetobacter xylinus strain ATCC 53524, J. Appl. Microbiol., 107(2), 576-583 (2009).

Oikawa, T., Ohtori, T. and Ameyama, M., Production of Cellulose from D-Mannitol by Acetobacter xylinum KU-1, Biosci. Biotechnol. Biochem., 59(2), 331-332 (1995).

Olijve, W. and Kok, J. J.: An analysis of the growth of Gluconobacter oxydans in chemostat cultures, Arch. Microbiol., 121(3), 291-297 (1979).

Orth, J. D., Thiele, I. and Palsson, B. Ø., What is flux balance analysis?, Nat. Biotechnol., 28(3), 245-248 (2010).

Orth J, F. R. P. B., Reconstruction and Use of Microbial Metabolic Networks: the Core Escherichia coli Metabolic Model as an Educational Guide, EcoSal Plus. Available from: http://www.asmscience.org/content/journal/ecosalplus/10.1128/ecosalplus.10.2.1. (2010).

Paley, S. M., Latendresse, M. and Karp, P. D., Regulatory network operations in the Pathway Tools software, BMC Bioinformatics, 13(1), 243 (2012).

Palsson, B. O., Systems Biology: Properties of Reconstructed Networks. (2006).

Raman, K. and Chandra, N., Flux balance analysis of biological systems: Applications and challenges, Brief. Bioinform., 10(4), 435-449 (2009).

Ramana, K., Tomar, A. and Singh, L., Effect of various carbon and nitrogen sources on cellulose synthesis by Acetobacter xylinum, World J. Microbiol. Biotechnol., 16, 245-248 (2000).

Reed, J. L., Shrinking the Metabolic Solution Space Using Experimental Datasets, PLoS Comput Biol, 8(8), e1002662 (2012).

Ross, P., Mayer, R. and Benziman, M., Cellulose biosynthesis and function in bacteria., Microbiol. Rev., 55(1), 35-58 (1991).

Ruka, D. R., Simon, G. P. and Dean, K. M., Altering the growth conditions of Gluconacetobacter xylinus to maximize the yield of bacterial cellulose, Carbohydr. Polym., 89(2), 613-622 (2012).

Scheer, M., Grote, A., Chang, A., Schomburg, I., Munaretto, C., Rother, M., Söhngen, C., Stelzer, M., Thiele, J. and Schomburg, D., BRENDA, the enzyme information system in 2011, Nucleic Acids Res., 39(suppl 1), D670-D676 (2011).

Schellenberger, J., Que, R., Fleming, R. M. T., Thiele, I., Orth, J. D., Feist, A. M., Zielinski, D. C., Bordbar, A., Lewis, N. E., Rahmanian, S., Kang, J., Hyduke, D. R. and Palsson, B. O., Quantitative prediction of cellular metabolism with constraint-based models: the COBRA Toolbox v2.0, Nat. Protoc., 6(9), 1290-1307 (2011).

Shimizu, K., Toward systematic metabolic engineering based on the analysis of metabolic regulation by the integration of different levels of information, Biochem. Eng. J., 46(3), 235-251 (2009).

Simeonidis, E. and Price, N., Genome-scale modeling for metabolic engineering, J. Ind. Microbiol. Biotechnol., 42(3), 327-338 (2015).

Terzer, M., Maynard, N. D., Covert, M. W. and Stelling, J., Genome-scale metabolic networks, Wiley Interdiscip. Rev. Biol. Med., 1(3), 285-297 (2009).

Thiele, I. and Palsson, B. O., A protocol for generating a high-quality genome-scale metabolic reconstruction, Nat. Protoc., 5(1), 93-121 (2010).

Velasco-Bedrán, H. and López-Isunza, F., The unified metabolism of Gluconacetobacter entanii in continuous and batch processes, Process Biochem., 42(8), 1180-1190 (2007).

Wiechert, W., Modeling and simulation: tools for metabolic engineering, J. Biotechnol., 94(1), 37-63 (2002).

Yamada, Y., Yukphan, P., Lan Vu, H. T., Muramatsu, Y., Ochaikul, D., Tanasupawat, S. and Nakagawa, Y., Description of *Komagataeibacter* gen. nov., with proposals of new combinations (*Acetobacteraceae*), J. Gen. Appl. Microbiol., 58(5), 397-404 (2012).

Yamanaka, S., Watanabe, K., Kitamura, N., Iguchi, M., Mitsuhashi, S., Nishi, Y. and Uryu, M., The structure

and mechanical properties of sheets prepared from bacterial cellulose, J. Mater. Sci., 24(9), 3141-3145 (1989).

Zeng, X., Liu, J., Chen, J., Wang, Q., Li, Z. and Wang, H., Screening of the common culture conditions affecting crystallinity of bacterial cellulose, J. Ind. Microbiol. Biotechnol., 38(12), 1993-1999 (2011).

Zhang, C. and Hua, Q., Applications of Genome-Scale Metabolic Models in Biotechnology and Systems Medicine, Front. Physiol., 6, 413 (2015).

Zhong, C., Zhang, G.-C., Liu, M., Zheng, X.-T., Han, P.-P. and Jia, S.-R., Metabolic flux analysis of Gluconacetobacter xylinus for bacterial cellulose production, Appl. Microbiol. Biotechnol., 97(14), 6189-6199 (2013).

Zhong, C., Li, F., Liu, M., Yang, X.-N., Zhu, H.-X., Jia, Y.-Y., Jia, S.-R. and Piergiovanni, L., Revealing Differences in Metabolic Flux Distributions between a Mutant Strain and Its Parent Strain Gluconacetobacter xylinus CGMCC 2955, PLoS One, 9(6), e98772 (2014).

APPENDIX

Table A1. List of all biochemical reactions of the core model network.

Abbrev	RxN	Description	Equation	Equation	EC	GENE	Subsistem
v1_gli		glucose transport in/out via diffusion reversible	GLC_x -> GLC	D-glucose_out ->D-glucose			
v2_o2		O2 transport via diffusion	O2_x -> O2	Oxygen_out <=> Oxygen			
v3_co2		CO2 transport via diffusion	CO2_x <-> CO2	Carbon dioxide_out <=>Carbon dioxide			
v4_bio		biomass transport out	BIOMASS -> BIOMASS_x	biomass -> biomass_out			
v5_cell		cellulose transport out	CELL -> CELL_x	cellulose ->Cellulose_out			
v6_ mann		mannitol transport in/out via diffusion reversible	MANN_x -> MANN	mannitol_out-> mannitol			
v7_nh4		nitrogen transport	NH4_x <-> NH4	ammonium_out<=> ammonium			
v8_glyc		glycerol transport in/out via diffusion reversible	GLYC_x -> GLYC	Glycerol_out -> Glycerol			
v9_h2o		water transport	H2O_x <-> H2O	water_out <-> water			
v10_ glcn		gluconate - gluconic acid transport	GLCN -> GLCN_x	Gluconate -> Gluconate_out			
v11_h		proton transport	H_x <-> H	hidrogen_out <-> hidrogen			
v12_pi		phosphate transport	PI_x + ATP + H2O -> PI + ADP + H	phosphate_out + atp + water <-> phosphate + adp + proton			
v13	R00299	glucokinase	GLC + ATP -> ADP + G6P	ATP + D-glucose <->ADP + D-Glucose 6-phosphate	2.7.1.2	GXY_05501, GXY_13683(putative)	Glycolysis/Gluconeogenesis
v14	R00741	phosphoglucoisomerase	G6P <-> F6P	D-Glucose 6-phosphate <=> D-Fructose 6-phosphate	5.3.1.9	GXY_02166	Glycolysis/Gluconeogenesis
v15	R00762	fructose difosfatos	FDP + H2O -> F6P + PI	Fructose 1,6-bisphosphate + H2O => D-Fructose 6-phosphate + Orthophosphate	3.1.3.11	GXY_08300 (glpX)	Glycolysis/Gluconeogenesis
v16	R01068	fructose-bisphosphate aldolase	FDP <-> DHAP + G3P	Fructose 1,6-bisphosphate <=> Glycerone phosphate + D-Glyceraldehyde 3-phosphate	4.1.2.13	GXY_08305, GXY_09124	Glycolysis/Gluconeogenesis
v17	R01015	triosephosphate isomerase	DHAP <-> G3P	Glycerone phosphate<-> D-Glyceraldehyde 3-phosphate	5.3.1.1	GXY_10284	Glycolysis/Gluconeogenesis
v18	R01061	glyceraldehyde 3-phosphate dehydrogenase	G3P + NAD + PI -> 13-DPG + NADH_x + H	D-Glyceraldehyde 3-phosphate + NAD+ + Orthophosphate<=> 3-Phospho-D-glyceroyl phosphate + NADH + H+	1.2.1.12	GXY_04003	Glycolysis/Gluconeogenesis
v19	R01512	phosphoglycerate kinase	13-DPG + ADP + PI <-> ATP + 3-PG	3-Phospho-D-glyceroyl phosphate + ADP <-> ATP + 3-Phospho-D-glycerate	2.7.2.3	GXY_03998 (pgk)	Glycolysis/Gluconeogenesis
v20	R01518	phosphoglycerate mutase	3-PG <-> 2-PG	3-Phospho-D-glycerate <=> 2-Phospho-D-glycerate	5.4.2.1	GXY_02671,GXY_12768	Glycolysis/Gluconeogenesis
v21	R00658	phosphopyruvate hydratase/enolase	2-PG <-> PEP + H2O	2-Phospho-D-glycerate <=> Phosphoenolpyruvate + H2O	4.2.1.11	GXY_10254 (eno)	Glycolysis/Gluconeogenesis
v22	R00200	pyruvate kinase	PEP + ADP + H -> ATP + PYR	Phosphoenolpyruvate + ADP => ATP + Pyruvate	2.7.1.40	GXY_00359	Glycolysis/Gluconeogenesis
v23	R00209	pyruvate dehydrogenase complex	PYR + NAD + COA -> ACCOA_x + NADH_x + CO2	Pyruvate + NAD+ + CoenzimaA<=> Acetyl-CoA + CO2 + NADH + H+	(2.3.1.12 and 1.8.1.4 and 1.2.4.1)	(GXY_16242 OR GXY_10329 OR GXY_07680) - (GXY_03931 OR(GXY_03931 AND GXY_03943) - (GXY_15912 OR (ilvH AND GXY_00049) OR (GXY_10324 AND GXY_10319) OR (GXY_13548 OR GXY_15937)	Glycolysis/Gluconeogenesis
v24	R00206	pyruvate phosphate dikinase	PYR + ATP + PI -> AMP + PEP + PPI	ATP + Pyruvate + Orthophosphate <=> AMP + Phosphoenolpyruvate + Diphosphate	2.7.9.1	GXY_08205	Glycolysis/Gluconeogenesis
v25	R00217	oxaloacetate decarboxylase	OAA + ADP + PI -> PYR + ATP + CO2	Oxaloacetate + ADP + phosphate -> pyruvate + ATP + CO2	4.1.1.3		Glycolysis/Gluconeogenesis
v26	R00345	phosphoenolpyruvate carboxylase	PEP + H2O + CO2 -> OAA + PI + H	Phosphoenolpyruvate + H2O + CO2 -> + Oxaloacetate + Orthophosphate	4.1.1.31	GXY_12143	Glycolysis/Gluconeogenesis
v27	R08639	phosphoglucomutase	G6P -> G1P	D-Glucose 6-phosphate -> D-Glucose 1-phosphate	5.4.2.2	GXY_09809	Glycolysis/Gluconeogenesis

Abbrev	RxN	Description	Equation	Equation	EC	GENE	Subsistem
v28	R00289	uridine glucose pyrophosphorylase	G1P + UTP + H -> UDPG + PPI	D-Glucose 1-phosphate + UTP + H <=> UDP-glucose + Diphosphate	2.7.7.9	GXY_10109	Starch and sucrose metabolism
v29	R02889	cellulose - UDP forming	UDPG -> UDP + CELL	UDP-glucose-> UDP + Cellulose	2.4.1.12	GXY_04277, GXY_08869	Starch and sucrose metabolism
v30			GLC + Q8 + H2O -> GLCN + Q8H2	D-Glucose + Ubiquinone + H2O => Gluconate + Ubiquinol			
v31	R01737	gluconokinase/gluconate dehydrogenase	GLCN + ATP -> ADP + 6-PGC + H	D-Gluconic acid/gluconate + atp ->ADP + 6-Phospho-D-gluconate	2.7.1.12	GXY_02201,GXY_12403	pentose phosphate
v32	R00835	glucose-6-phosphate dehydrogenase	G6P + NADP_x <-> 6-PGL + NADPH	D-Glucose 6-phosphate + NADP+ <=> D-Glucono-1,5-lactone 6-phosphate + NADPH + H+	1.1.1.49	GXY_01616,GXY_02176,GXY_11509	pentose phosphate
v33	R02035	6-phosphogluconolactonase	6-PGL + H2O -> 6-PGC	D-Glucono-1,5-lactone 6-phosphate + H2O => 6-Phospho-D-gluconate	3.1.1.31	GXY_02191,GXY_10154	pentose phosphate
v34	R01528	6-phosphogluconate dehydrogenase	6-PGC + NADP_x -> RU5P + CO2 + NADPH	6-Phospho-D-gluconate + NADP+ -> D-Ribulose 5-phosphate + CO2 + NADPH	1.1.1.44	GXY_04594	pentose phosphate
v35	R02036	phosphogluconate dehydratase	6-PGC -> 2-DDG6P + H2O	6-Phospho-D-gluconate => 2-Dehydro-3-deoxy-6-phospho-D-gluconate + H2O	4.2.1.12	GXY_03863	pentose phosphate
v36	R05605	2-dehydro-3-deoxyphosphogluconate aldolase	2-DDG6P -> G3P + PYR	2-Dehydro-3-deoxy-6-phospho-D-gluconate => D-Glyceraldehyde 3-phosphate + Pyruvate	4.1.2.14	GXY_03858	pentose phosphate
v37	R01529	epimerase	RU5P <-> XU5P	D-Ribulose 5-phosphate <=> D-Xylulose 5-phosphate	5.1.3.1		pentose phosphate
v38	R01056	isomerase	RU5P <-> R5P	D-Ribulose 5-phosphate<=> D-Ribose 5-phosphate	5.3.1.6	GXY_02196	pentose phosphate
v39	R01827	transaldolase	S7P + G3P <-> E4P + F6P	Sedoheptulose 7-phosphate + D-Glyceraldehyde 3-phosphate => D-Erythrose 4-phosphate + D-Fructose 6-phosphate	2.2.1.2	GXY_02166	pentose phosphate
v40	R01641	transketolase	R5P + XU5P <-> S7P + G3P	D-Ribose 5-phosphate + D-Xylulose 5-phosphate =>Sedoheptulose 7-phosphate + D-Glyceraldehyde 3-phosphate	2.2.1.1	GXY_02161,GXY_04008	pentose phosphate
v41	R01067	transketolase	E4P + XU5P <-> F6P + G3P	D-Erythrose 4-phosphate + D-Xylulose 5-phosphate <=>D-Fructose 6-phosphate + D-Glyceraldehyde 3-phosphate	2.2.1.1	GXY_02161,GXY_04008	pentose phosphate
v42	R00868	mannitol 2-dehydrogenase	MANN + NAD <-> FRU + NADH_x + H	Mannitol + NAD+ <=> D-Fructose + NADH + H+	1.1.1.67	GXY_02161	manitol
v43	R00760	fructokinase	FRU + ATP -> ADP + F6P + H	ATP + D-Fructose => ADP + D-Fructose 6-phosphate	2.7.1.4	GXY_10569	
v44	R00847	glycerol kinase	GLYC + ATP -> ADP + GLYC3P	Glycerol + ATP=> ADP + Glycerol 3-phosphate	2.7.1.30	GXY_08295	Glycerophospholipid metabolism
v45	R00842	glycerol-3-phosphate dehydrogenase	GLYC3P + NAD <-> DHAP + NADH_x + H	Glycerol 3-phosphate + NAD<=> Glycerone phosphate + NADH	1.1.1.94	GXY_04966	Glycerophospholipid metabolism
v46	R00351	citrate synthase	ACCOA_x + H2O + OAA -> CIT + COA + H	Acetyl-CoA + H2O + Oxaloacetate=> Citrate + CoA	2.3.3.1	GXY_10922	TCA cycle
v47	R01325	aconitate hydratase 1	CIT -> ACON-C + H2O	Citrate => cis-Aconitate + H2O	4.2.1.3	GXY_01403	TCA cycle
v48	R01900	aconitate hydratase 2	ACON-C + H2O <-> ICIT	cis-Aconitate + H2O <=> Isocitrate	4.2.1.3	GXY_01403	TCA cycle
v49	R00267	isocitrate dehydrogenase	ICIT + NADP_x <-> AKG + CO2 + NADPH + H	Isocitrate + NADP+ <=> 2-Oxoglutarate + CO2 + NADPH + H+	1.1.1.42	GXY_08180	TCA cycle
v50	R01197	2-oxoglutarate synthase	AKG + NAD + COA -> SUCCOA + NADH_x + CO2		1.2.7.3		TCA cycle
v51	R00405	succinyl-CoA synthetase	SUCCOA + ADP + PI <-> ATP + SUCC + COA	ADP + orthophosphate + succinyl-CoA => ATP + succinate + CoA	6.2.1.5	GXY_05758, GXY_05763	TCA cycle
v52	R00408	Succinate dehydrogenase	SUCC + FAD <-> FADH2 + FUM	Succinate + FAD <=> FADH2 + Fumarate	1.3.99.1	GXY_01598 - sdhB	TCA cycle
v53	R01082	fumarase	FUM + H2O <-> MAL-L	Fumarate + H2O<-> (S)-Malate	4.2.1.2	GXY_13863, GXY_02031	TCA cycle
v54	R00342	malate dehydrogenase	MAL-L + NAD <-> NADH_x + OAA + H	(S)-Malate + NAD+ => Oxaloacetate + NADH2 + H+	1.1.1.37		TCA cycle
v55	R00253	glutamine synthetase	ATP + GLU-L + NH4 -> ADP + PI + GLN-L + H	ATP + L-Glutamate + NH4 -> ADP + Orthophosphate + L-Glutamine	6.3.1.2	GXY_02336	nitrogen metabolism
v56	R00256	glutaminase	GLN-L + H2O -> GLU-L + NH4	L-Glutamine + Water => L-Glutamate + NH4	3.5.1.2	GXY_12733; carB	nitrogen metabolism
v57	R00114	glutamate synthase	GLN-L + AKG + NADPH + H -> 2GLU-L + NADP_x	L-Glutamine + 2-Oxoglutarate + NADPH + H+ => L-Glutamate + NADP+	1.4.1.13	GXY_04844, gxy_04839	nitrogen metabolism
v58			GLN-L_x + H_x <-> GLN-L + H	L-Glutamine_out + proton => L-Glutamine + proton			transport
v59			GLU-L_x + H_x <-> GLU-L + H	L-Glutamate_out + proton => L-Glutamate + proton			transport
v60		adenylate kinase	AMP + ATP <-> 2ADP	AMP + ATP <-> 2ADP	2.7.4.3	GXY_12943	purine metabolism
v61		ATP maintenance requirement	ATP + H2O -> ADP + PI + H	ATP + H2O -> ADP + PI + H			
v62		ATP synthase - Complex V	ADP + PI + 4H_x -> ATP + H2O + 3H	ADP + PI + 4H_x -> ATP + H2O + 3H	3.6.3.14	GXY_00619, GXY_00624, GXY_00629, GXY_00634, GXY_15649, GXY_15672, GXY_15677, GXY_15682	oxidative phosphorilation
v63		inorganic diphosphatase	PPI + H2O -> 2PI + H	Diphosphate + H2O -> 2 ortophosphate + H	3.6.1.1	GXY_01896	

Abbrev	RxN	Description	Equation	Equation	EC	GENE	Subsistem
v64		NAD transhydrogenase	NAD + NADPH -> NADH_x + NADP_x	NAD + NADPH + H-> NADH + NADP+H_out	1.6.1.2		
v65		nucleoside-triphosphatase (UTP)	UTP + H2O -> UDP + H + PI	UTP + H2O -> UDP + H + PI	3.6.1.5		purine metabolism
v66		nucleoside-diphosphate kinase (ATP:UDP)	ATP + UDP -> ADP + UTP	ATP + UDP -> ADP + UTP	2.7.4.6	ndk	purine metabolism
v67		Complex I (NADH desidrogenase)	Q8 + NADH_x + 5H -> Q8H2 + NAD + 4H_x	Ubiquinone + NADH + 5H => Ubiquinol + NAD + 4H	1.6.5.3	GXY_08325,GXY_11983,GXY_11988,GXY_11993,GXY_12583,GXY_15579	oxidative phosphorilation
v68		Complex II (succinate desidrogenase)	Q8 + SUCC -> Q8H2 + FUM	Ubiquinone + Succinate -> Ubiquinol + Fumarate	1.3.5.1		oxidative phosphorilation
v69		Ubiquinol Oxidase (citocromo bd oxidase)	2Q8H2 + 4H + O2 -> 2Q8 + 2H2O + 4H_x	2Ubiquinol + 4H + Oxygen => 2Ubiquinone + 2H2O + 4H_out	1.10.3.10	GXY_05121,GXY_05126,GXY_05131,GXY_05136	oxidative phosphorilation
v70		Complex IV (citocromo c oxidase)	O2 + 4FERROCYTOCHROME + 4H -> 4FERRICYTOCHROME + 2H2O + 4H_x	Oxygen + 4 reduced-cytochrome-c => 4oxidized-cytochrome-c + 2H2O + 4H_out	1.9.3.1	GXY_04894,GXY_07135	oxidative phosphorilation
v71		Complex III (citocromo bc1)	Q8H2 + 2FERRICYTOCHROME + 2H -> Q8 + 2FERROCYTOCHROME + 4H_x	Ubiquinol + 2 oxidized-cytochrome-c -> Ubiquinone + 2 reduced-cytochrome-c	1.10.2.2	GXY_00569,GXY_00574,GXY_16474	oxidative phosphorilation
v72			NADH_x + 0.5O2 + 2.5ADP + 2.5PI + 3.5H -> 3.5H2O + NAD + 2.5ATP	NADH_x + 0.5O2 + 2.5ADP + 2.5PI + 3.5H -> 3.5H2O + NAD + 2.5ATP			oxidative phosphorilation
v73			FADH2 + 0.5O2 + 1.5ADP + 1.5PI + 2.5H -> 2.5H2O + FAD + 1.5ATP	FADH2 + 0.5O2 + 1.5ADP + 1.5PI + 2.5H -> 2.5H2O + FAD + 1.5ATP			
v74		biomass reaction	41.257ATP + 0.205G6P + 0.0709F6P + 0.8977R5P + 0.8977E4P + 0.129G3P + 1.496*3-PG + 0.5191PEP + 28.328PYR + 3.747ACCOA_x + 1.078AKG + 1.786OAA + 1.822NADPH + 3.547NAD + 41.257H2O -> 41.257ADP + 41.257PI + 3.747CoA+ 1.822NADP + 46.626H + BIOMASS				biomass

BIOMASS COMPOSITION

Metabolites	**Coefficient**
NADPH	-1.822
D-Erythrose4-phosphate	-0.8977
NADH	3.547
Phosphoenolpyruvate	-0.5191
NADP	1.822
NAD	-3.547
H2O	-41.257
Acetyl-CoA	-3.747
ADP	41.257
CoA	3.747
ATP	-41.257
Pyruvate	-2.832
3-Phosphoglycerate	-1.496
Oxaloacetate	-1.786
Phosphate	41.257
D-fructose-6-phosphate	-0.0709
ribose-5-phosphate	-0.8977
H+	46.626
Glyceraldehyde3-phosphate	-0.129
2-Oxoglutarate	-1.078
D-glucose-6-phosphate	-0.205
Biomass	1

EXCHANGE REACTIONS

EX_co2(e)	CO2 exchange	co2_out[e] <=>
EX_glc-D(e)	glucose exchange	glc-D_out[e] <=>
EX_glyc(e)	glycerol exchange	glyc_out[e] <=>
EX_h(e)	H+ exchange	h_out[e] <=>
EX_h2o(e)	H2O exchange	h2o_out[e] <=>
EX_mann(e)	mannitol exchange	mann_out[e] <=>
EX_nh4(e)	NH4 exchange	nh4_out[e] <=>
EX_pi(e)	phosphate exchange	pi_out[e] <=>

Abbrev	RxN	Description	Equation	Equation	EC	GENE	Subsistem
		EX_o2(e)		oxygen exchange		o2_out[e] <=>	
		DEMAND REACTIONS					
		DM_g6p		Glucose -6-phosphate demand			
		DM_f6p		Fructose-6-phosphate demand			
		DM_r5p		Ribose-5-phosphate demand			
		DM_e4p		Erythose-4-phosphate demand			
		DM_g3p		Glyceraldehyde -3-phosphate demand			
		DM_3-pg		3-Phospho-D-glycerate demand			
		DM_pep		Phosphooenolpyruvate demand			
		DM_pyr		Pyruvate demand			
		DM_accoa		Acetyl-CoA demand			
		DM_akg		2-oxoglutaratedemand			
		DM_oaa		Oxaloacetate demand			

Table A2. List of all metabolites of the core model network.

Abbrev.	Description	Neutral Formula	Charged formula	Charge	KEGG ID	Compart-ment	PubChem ID
13dpg	3-Phospho-D-glyceroyl phosphate	C3H8O10P2	C3H4O10P2	-4	C00236	cytosol	3535
2ddg6p	2-Dehydro-3-deoxy-6-phospho-D-gluconate	C6H11O9P	C6H8O9P	-3	c04442	cytosol	7071
2pg	D-Glycerate 2-phosphate	C3H7O7P	C3H4O7P	-3	C00631	cytosol	3904
3pg	3-Phospho-D-glycerate	C3H7O7P	C3H4O7P	-3	C00197	cytosol	3497
6pgc	6-Phospho-D-gluconate	C6H13O10P	C6H10O10P	-3	c00345	cytosol	3638
6pgl	D-glucono-1,5-lactone-6-phosphate	C6H11O9P	C6H9O9P	-2	c01236	cytosol	4457
ac	Acetate	C2H4O2	C2H3O2	-1	C00033	cytosol	3335
acald	Acetaldehyde	C2H4O	C2H4O	0	C00084	cytosol	3384
accoa	Acetyl-CoA	C23H38N7O17P3S	C23H34N7O17P3S	-4	C00024	cytosol	3326
acon-C	Cis-Aconitate	C6H6O6	C6H3O6	-3	C00417	cytosol	3707
actp	Acetyl phosphate	C2H3O5P	C2H5O5P	-2	C00227	cytosol	3527
adp	ADP	C10H15N5O10P2	C10H12N5O10P2	-3	C00008	cytosol	3310
akg	2-oxoglutarate	C5H6O5	C5H4O5	-2	C00026	cytosol	3328
amp	AMP	C10H14N5O7P	C10H12N5O7P	-2	c00020	cytosol	3322
atp	ATP	C10H16N5O13P3	C10H12N5O13P3	-4	C00002	cytosol	3304
biomass	Biomass			0	[]	cytosol	[]
biomass_out	Biomass_out			0	[]	extracellular	[]
cell	Cellulose or 1,4-beta-D-glucan	C6H10O5	C6H10O5	0	c00760	cytosol	4022
cell_out	Cellulose or 1,4-beta-D-glucan	C6H10O5	C6H10O5	0	c00760	extracellular	4022
cit	Citrate	C6H8O7	C6H5O7	-3	C00158	cytosol	3458
co2	carbon dioxide	CO2	CO2	0	C00011	cytosol	3313
co2_out	carbon dioxide_out	CO2	CO2	0	C00011	extracellular	3313
CoA	Coenzime A	C21H36N7O16P3S	C21H32N7O16P3S	-4	C00010	cytosol	3312
dha	Glycerone or Dihydroxyacetone	C3H6O3	C3H6O3	0	c00184	cytosol	3484
dhap	Glycerone phosphate/ Dihydroxyacetone phosphate	C3H7O6P	C3H5O6P	-2	C00111	cytosol	3411
e4p	D-Erythrose 4-phosphate	C4H9O7P	C4H7O7P	-2	c00085	cytosol	3574
f6p	D-Fructose 6-phosphate	C6H13O9P	C6H11O9P	-2	c00016	cytosol	3385
fad	Flavin adenine dinucleotide	C27H33N9O15P2	C27H31N9O15P2	-2	C01352	cytosol	3318
fadh2	FADH2	C27H35N9O15P2	C27H33N9O15P2	-2	C00354	cytosol	4556
fdp	Fructose 1,6-bisphosphate	C6H14O12P2	C6H10O12P2	-4	C00125	cytosol	3647
Ferricytochrome c	Oxidized cytochrome c	C42H44FeN8O8S2R4	C42H44FeN8O8S2R4	0	C00126	cytosol	3425
Ferrocytochrome c	Reduced cytochrome c	C42H44FeN8O8S2R4	C42H44FeN8O8S2R4	0	c00095	cytosol	3426
fru	D-fructose	C6H12O6	C6H12O6	0	C00122	cytosol	3395
fum	fumarate	C4H4O4	C4H2O4	-2	C00103	cytosol	3422
g1p	D-glucose 1-phosphate	C6H13O9P	C6H11O9P	-2	C00118	cytosol	3403
g3p	Glyceraldehyde 3-phosphate	C3H7O6P	C3H5O6P	-2	C00092	cytosol	3418
g6p	D-glucose 6-phosphate	C6H13O9P	C6H11O9P	-2	c00031	cytosol	3392

Abbrev.	Description	Neutral Formula	Charged formula	Charge	KEGG ID	Compart-ment	PubChem ID
glc-D	D-glucose	C6H12O6	C6H12O6	0	c00031	extracellular	3333
glc-D_out	D-glucose_out	C6H12O6	C6H12O6	0	c00257	cytosol	3333
glcn	D-gluconic acid or D-gluconate	C6H12O7	C6H11O7	-1	c00257	cytosol	3556
glcn_out	D-gluconic acid or D-gluconate	C6H12O7	C6H11O7	-1	C00064	cytosol	3556
gln-L	L-glutamine	C5H10N2O3	C5H10N2O3	0	C00025	cytosol	3364
glu-L	L-glutamate	C5H8NO4	C5H9NO4	-1	c00116	cytosol	3327
glyc	Glycerol or 1,2,3-Trihydroxypropane	C3H8O3	C3H8O3	0	c00116	extracellular	3416
glyc_out	Glycerol or 1,2,3-Trihydroxypropane	C3H8O3	C3H8O3	0	c00093	cytosol	3416
glyc3p	Glycerol 3 -phosphate	C3H9O6P	C3H7O6P	-2	C00080	cytosol	3393
h	H+ /proton	H	H	1	C00080	extracellular	3380
h_out	H+/proton_out	H	H	1	C00001	cytosol	3380
h2o	water	H2O	H2O	0	C00001	extracellular	3303
h2o_out	water_out	H2O	H2O	0	c00311	cytosol	3303
icit	Isocitrate	C6H8O7	C6H5O7	-3	C15972	cytosol	3605
mal	(S)-Malate / Malic Acid	C4H6O5	C4H4O5	-2	c00392	cytosol	3449
mann	D-mannitol	C6H14O6	C6H14O6	0	c00392	extracellular	3682
mann_out	D-mannitol_out	C6H14O6	C6H14O6	0	C00003	cytosol	3682
nad	Nicotinamide adenine dinucleotide	C21H28N7O14P2	C21H26N7O14P2	-1	C00004	cytosol	3305
nadh	Nicotinamide adenine dinucleotide - reduced	C21H29N7O14P2	C21H27N7O14P2	-2	C00006	cytosol	3306
nadp	Nicotinamide adenine dinucleotide phosphate	C21H28N7O17P3	C21H25N7O17P3	-3	C00005	cytosol	3307
nadph	Nicotinamide adenine dinucleotide phosphate - reduced	C21H30N7O17P3	C21H26N7O17P3	-4	C01342	cytosol	3308
nh4	Ammonium	NH3	NH4	1	C01342	extracellular	4547
nh4_out	Ammonium_out	NH3	NH4	1	c00007	cytosol	4547
o2	Oxygen	O2	O2	0	c00007	extracellular	3309
o2_out	Oxygen_out	O2	O2	0	C00036	cytosol	3309
oaa	Oxaloacetate	C4H4O5	C4H2O5	-2	C00074	cytosol	3338
pep	Phosphoenolpyruvate	C3H5O6P	C3H2O6P	-3	c00198	cytosol	3374
pgl	D-glucono-1,5-lactone / Gluconic lactone	C6H10O6	C6H10O6	0	C00009	cytosol	3498
pi	orthophosphate	H3O4P	HO4P	-2	c00013	cytosol	3311
ppi	Diphosphate or pirofosfato	H4P2O7	HO7P2	-3	C00022	cytosol	3315
pyr	pyruvate	C3H4O3	C3H3O3	-1	c00399	cytosol	3324
q8	Ubiquinone	C14H18O4	C14H18O4	0	c00390	cytosol	3689
q8h2	Ubiquinol	C14H20O4	C14H20O4	0	C00117	cytosol	3680
r5p	D-Ribose 5-phosphate	C5H11O8P	C5H9O8P	-2	C00199	cytosol	3417
ru5p	D-Ribulose 5-phosphate	C5H11O8P	C5H9O8P	-2	C00281	cytosol	3499
s7p	Sedoheptulose 7-phosphate	C7H15O10P	C7H13O10P	-2	C05382	cytosol	7756
succ	succinate	C4H6O4	C4H4O4	-2	C00042	cytosol	3344
succoa	Succinyl-CoA	C25H40N7O19P3S	C25H35N7O19P3S	-5	C00091	cytosol	3391
udp	Uridine 5'-diphosphate	C9H14N2O12P2	C9H11N2O12P2	-3	c00015	cytosol	3317
udpg	UDPglucose	C15H24N2O17P2	C15H22N2O17P2	-2	c00029	cytosol	3331
utp	Uridine triphosphate	C9H15N2O15P3	C9H11N2O15P3	-4	C00075	cytosol	3375
xu5p	D-Xylulose 5-phosphate	C5H11O8P	C5H9O8P	-2	C00231	cytosol	3530